Journal of Inorganic and Organometallic Polymers and Materials (2019) 29:1874–1885
https://doi.org/10.1007/s10904-019-01148-6

A Novel Magnetic Cd(II) Ion-Imprinted Polymer as a Selective Sorbent for the Removal of Cadmium Ions from Aqueous Solution

Hongpeng Wang[1] · Yuecheng Lin[1] · Yin Li[1] · Anudari Dolgormaa[1] · Hui Fang[1] · Lin Guo[2] · Jun Huang[1] · Junxing Yang[3]

Received: 24 February 2019 / Accepted: 4 April 2019 / Published online: 9 April 2019
© Springer Science+Business Media, LLC, part of Springer Nature 2019

Abstract
To improve the adsorption capacity of Cd(II) ions, Cd(II) ions were imprinted on the surface of aminoethyl chitosan (AECS), which was coated on Fe_3O_4@SiO_2 nanoparticles. A novel magnetic Cd(II) ion-imprinted polymer (Cd(II)-IIP) was synthesized, characterized, and applied to the selective separation of Cd(II) ions from aqueous solution. The adsorption–desorption properties and selectivity of Cd(II)-IIP and a non-imprinted polymer (Cd(II)-NIP) were investigated. The optimum pH and equilibrium binding time were established at pH 6.0 and 60 min, respectively. Kinetics studies demonstrated that the adsorption process proceeded according to a pseudo-first or second order model, while the adsorption isotherms agreed with the Langmuir model. The maximum adsorption capacities of Cd(II)-IIP and Cd(II)-NIP toward Cd(II) ions, as calculated by the Langmuir equation, at pH 6.0 and 25 °C were 26.1 and 6.7 mg/g, respectively. The imprinted polymer showed higher selectivity toward Cd(II) ions compared to the non-imprinted polymer. The relative selectivity factor (β_r) values of Cd(II)/Cu(II), Cd(II)/Cr(II), and Cd(II)/Pb(II) were 3.315, 3.875, and 2.061, respectively. In addition, Cd(II) ions adsorbed on the Cd(II)-IIP adsorbent could be easily released using 0.1 M HNO_3, thus showing good material stability and reusability. The adsorption capacity of Cd(II)-IIP was retained at 74% after undergoing six adsorption–desorption cycles.

Keywords Aminoethyl chitosan · Magnetic sorbent · Cd(II) imprinting · Adsorption · Heavy metal

1 Introduction

The painting, mining, and smelting industries have been reported to directly or indirectly discharge a large amount of heavy metal wastewater into aquatic systems, threatening the well-being of crops and humans [1–6]. Different treatment technologies have been developed for the removal of heavy metals from wastewater, including membrane separation, electrocoagulation, and chemical precipitation [7]. However, their application has been limited by high operational cost and large energy consumption [8].

The adsorption technology is widely used for the removal of heavy metals [9–13]. As a traditional adsorption material, activated carbon has a highly porous structure and large absorption capacity, but it demonstrates a poor selectivity against organic and inorganic compounds, and its fabrication and regeneration procedures are expensive [14, 15]. Similarly, ion-exchange resins are also cost-prohibitive and their performance is pH-dependent [16]. Their modern alternatives were reported recently, such as starch-based materials [17], porous glass beads [18], modified activated carbon [19] and lignocellulosic residues [20]. Even though these materials interact effectively with heavy metal ions, they cannot be easily separated and reused after the adsorption process. In contrast to these traditional adsorbents, magnetic nano-sized iron oxide particles are environmentally friendly [21], can interact quickly with adsorbates [22], and are easily separated from aqueous samples using an external magnetic field [23], and can be sustainable utilization without secondary

✉ Jun Huang
hjunlzr@163.com

✉ Junxing Yang
yangajx@igsnrr.ac.cn

[1] Zhejiang Provincial Key Lab for Chemical and Biological Processing Technology of Farm Product, School of Biological and Chemical Engineering, Zhejiang University of Science and Technology, Hangzhou 310023, People's Republic of China

[2] Department of Biological and Environmental Sciences, Texas A&M University, Commerce TX75428, USA

[3] Institute of Geographical Sciences and Natural Resources Research, Chinese Academy of Sciences, Beijing 100101, People's Republic of China

pollution. However, pure magnetic Fe_3O_4 nanoparticles have limitations such as spontaneous aggregation due to high surface energy, and the loss of super paramagnetism when exposed to air [24]. In order to obtain higher stability and larger surface area, several materials with high adsorption capacity for heavy metals have been developed. Zargoosh et al. [25] previously prepared a magnetic nanoadsorbent synthesized by the covalent immobilization of thiosalicylhydrazide on the surface of Fe_3O_4 nanoparticles. The particles were coated with functional groups to afford excellent physical and chemical properties. Molecular imprinting of chitosan on the surface of magnetic nanoparticles modifies the particle surface but retains the beneficial properties of the superparamagnetic particles [26–28]. Xi et al. [8] synthesized cadmium ion-imprinted polymers via precipitation polymerization using a dithizone/cadmium complex as template.

Currently, there is limited literature on chitosan-based imprinted composite adsorbents, and their competitive adsorption behavior in binary or multi-component aqueous solutions is not widely known. Moreover, our literature review has revealed no previous attempts to imprint aminoethyl chitosan on the surface of magnetic iron oxide nanoparticles. To improve the adsorption capacity of Cd(II) ions, chitosan was modified with 2-chloroethylamine hydrochloride to afford aminoethyl chitosan (AECS), which was then coated on $Fe_3O_4@SiO_2$ nanoparticles to give a novel material: $Fe_3O_4@SiO_2@$AECS. Cd(II) ion-imprinted polymer (Cd(II)-IIP) was obtained by first imprinting Cd(II) ions on the surface of $Fe_3O_4@SiO_2@$AECS, followed by acid removal. As shown in Fig. 1, the ion-imprinted (Cd(II)-IIP) and non-ion-imprinted (Cd(II)-NIP) materials were subsequently compared in terms of their adsorption behavior toward Cd(II) ions in water.

2 Materials and Methods

2.1 Materials

Chitosan was prepared using a previously reported method [29]. Ferric chloride ($FeCl_3{\cdot}6H_2O$), ferrous chloride ($FeCl_2{\cdot}4H_2O$), Span 80, liquid paraffin, ethyl orthosilicate, 2-chloroethylamine hydrochloride, ammonium hydroxide, glutaraldehyde (GD), cadmium nitrate, absolute ethanol, and nitric acid were purchased from Aladdin Reagent Co. Ltd. (Shanghai, China). The water used for extraction and analysis was distilled and deionized using a Milli-Q system from Millipore (Bedford, MA, USA). All chemicals were of analytical grade and used directly without further purification.

2.2 Synthesis of AECS

AECS was prepared using an improved procedure based on the method reported by Je et al. [30]. About 75 mL of 1 M aqueous 2-chloroethylamine hydrochloride was added dropwise into 1.5 g of chitosan under stirring at 65 °C. Next, 75 mL of 1 M NaOH was added dropwise into the chitosan solution and the mixture was stirred at 80 °C for 18 h. The

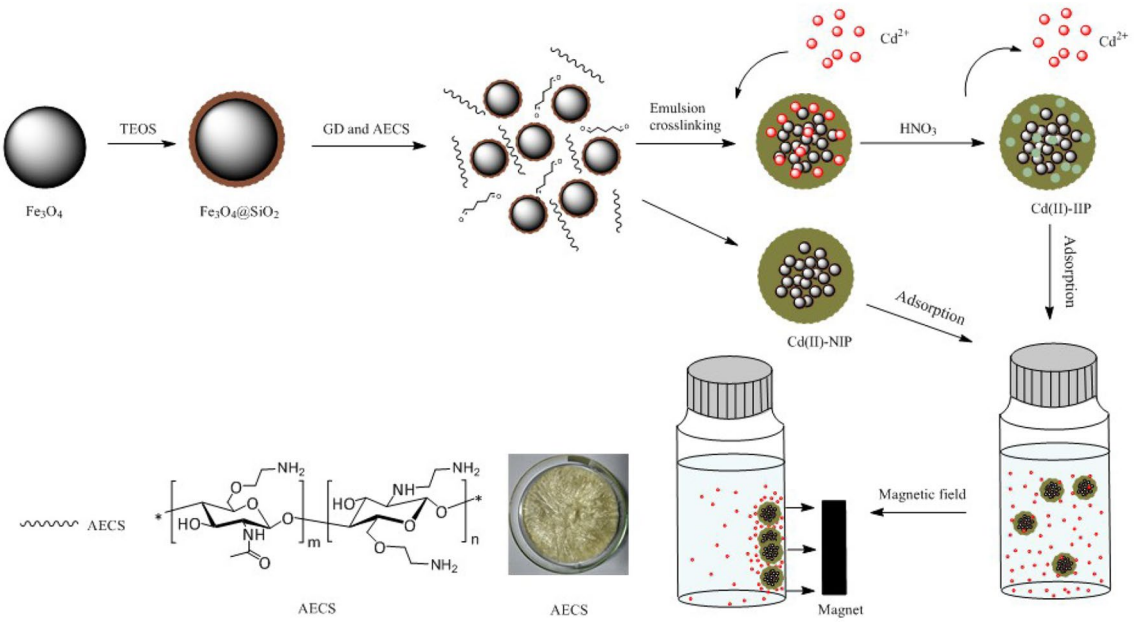

Fig. 1 Schematic diagram for the preparation of Cd(II) ion-imprinted polymer

product was then dialyzed with deionized water for 2 days, before undergoing vacuum lyophilization.

2.3 Preparation of Magnetic Fe_3O_4@SiO_2@AECS (Cd(II)-IIP and Cd(II)-NIP)

Magnetic Fe_3O_4 nanoparticles were prepared using a co-precipitation method [31]. Ferrous and ferric chloride (at a molar ratio of 2:1) were first dissolved in 100 mL of distilled water, followed by the dropwise addition of 15 mL of aqueous ammonia (29%). The mixture was then stirred under argon gas at 80 °C for 30 min. The resulting Fe_3O_4 nanoparticles were separated using an external magnetic field, washed several times with deionized water and anhydrous ethanol, and freeze-dried in vacuum.

Meanwhile, Fe_3O_4@SiO_2 nanoparticles were prepared based on the method reported by Stober et al. [32]. About 100 mg of Fe_3O_4 nanoparticles was dispersed in 100 mL of 80% ethanol solution under ultrasonication for about 10 min. The product was then separated using an external magnetic field, and washed several times with deionized water. The obtained nanoparticles were dispersed in 80 mL of anhydrous ethanol, mixed with 20 mL of water and 1 mL of aqueous ammonia. Next, about 2 mL of tetraethyl orthosilicate (TEOS) was slowly dripped into the solution, and the mixture was stirred at room temperature for 12 h. The obtained Fe_3O_4@SiO_2 particles were separated by magnetism, washed several times with deionized water and anhydrous ethanol, and freeze-dried in vacuum.

Subsequently, 50 mg of Fe_3O_4@SiO_2 was added into a solution consisting of 0.1 g of AECS and 10 mg of $Cd(NO_3)_2{\cdot}4H_2O$ dissolved in 3 mL of deionized water; the mixture was then stirred for 30 min under sonication. Next, 30 mL of liquid paraffin and 1 mL of Span 80 were added into the mixture and it was stirred at 300 rpm for 1 h to form a homogeneous solution. This was followed by adding 0.5 mL of 50% GD into the solution, and the mixture was stirred at 60 °C for 2.5 h. After centrifugal separation, the reaction product was washed with petroleum ether, ethanol, and deionized water until a neutral pH was achieved. Thereafter, the solid was repeatedly washed with 1 M HNO_3 until no Cd(II) ions were detected by flame atomic absorption spectrometry (FAAS). The obtained product (Cd(II)-IIP) was then washed with 1 M NaOH solution for 2 h until its pH became neutral, and it was freeze-dried in vacuum. Cd(II)-NIP was prepared using the same approach as that of Cd(II)-IIP but without introducing Cd(II) ions.

2.4 Characterization

The surface morphological images of magnetic Fe_3O_4 and the synthesized adsorbents were analyzed using X-ray diffraction (XRD) analysis (X'Pert PRO, PANalytical Company, Netherlands), transmission electron microscopy (TEM) (JEM-2010F, Jeol, Japan), scanning electron microscopy (SEM) (S-4700, Hitachi, Japan), optical microscopy (Moticam 2306, Mike Audi Industrial Group Co. Ltd., China). Complexation among the synthesized adsorbents was confirmed using Fourier transform infrared (FTIR, Vertex 70, Bruker Optik GmbH, Germany) and nuclear magnetic resonance (NMR) spectroscopy (ARX400, Bruker, Switzerland). The degree of deacetylation (DD) of chitosan was calculated according to a published method [33] using the H_2, H_3, H_4, H_5, H_6, and $H_{6'}$ (H_{2-6}) proton signals of both monomers and the integrals of the methyl group using the following equation:

$$\mathrm{DD}\,(\%) = \left\{1 - \left(\frac{1}{3}I_{\mathrm{CH_3}} \Big/ \frac{1}{6}I_{\mathrm{H_2-H_6}}\right)\right\} \times 100\% \quad (1)$$

Where, I_{CH_3} is the integral intensity of the CH_3 residue, and $I_{H_2\text{-}H_6}$ is the sum of the integral intensities of the H_2, H_3, H_4, H_5, H_6, and $H_{6'}$ protons. Magnetic behavior was analyzed by vibrating sample magnetometry (VSM, 4HF, ADE, USA). The concentration of metal ion in the solution was analyzed using flame atomic absorption spectrophotometry (AA-6300, Shimadzu Corporation, Japan). Thermal gravimetric analysis (TGA) was performed with an STA449 F3 DSC/DTA-TG analyzer (Netzsch, Germany) in the temperature range of 50–800 °C at a heating rate of 10 °C/min.

2.5 Adsorption Studies of the Adsorbents

2.5.1 Effect of pH on Adsorption Capacity

As AECS is more stable than chitosan in an acidic solution and metal ions are precipitated under alkaline conditions, the effect of pH on the adsorption capacity of the synthesized materials in acidic solution was investigated. Metal ion solutions at a different pH values (ranging from 2.0 to 6.0) were prepared and adjusted using 0.1 M HCl and NaOH solutions. The effect of pH on the Cd(II) ions adsorption process was studied over the pH range of 2.0–6.0, while fixing the initial Cd(II) ions concentration at 100 mg/L. About 5 mg each of Cd(II)-IIP and Cd(II)-NIP was added into several individual metal ion solutions, each measuring 10 mL in volume. The samples were shaken on an incubator shaker at 150 rpm and 25 °C for 6 h. After magnetic separation, the respective Cd(II) ions concentrations (C_e) were measured using flame atomic absorption spectrophotometry, and the corresponding adsorption capacities were calculated using the following equation [34]:

$$q_e = \frac{(C_0 - C_e)V}{m} \quad (2)$$

where, C_0 and C_e (mg/L) are the initial concentration and equilibrium concentration, respectively, V (L) is the volume

of the solution, m (g) is the weight of the adsorbent, and q_e (mg/g) is the equilibrium adsorption capacity.

2.5.2 Adsorption Kinetics

To study the adsorption capacity of the newly synthesized adsorbents, a test solution containing 10 mL of Cd(II) ion solution (at a concentration of 100 mg/L) and 5 mg of either Cd(II)-IIP or Cd(II)-NIP was used. The solution was adjusted to pH 6.0 using 0.1 M HCl and NaOH solutions. The test mixtures were shaken at 150 rpm and 25 °C, and sampling was performed at different time intervals until the absorption process reached equilibrium. After undergoing magnetic separation, the adsorption capacity q_e was determined using FAAS.

2.5.3 Adsorption Isotherm

Cd(II) ion solutions with different initial concentrations, i.e. 0, 5, 10, 25, 50, 100, 250, and 500 mg/L, were prepared. Either 5 mg of Cd(II)-IIP or Cd(II)-NIP was dispersed into Cd(II) ion solutions at different concentrations (each measuring 10 mL in volume), and their pH was adjusted to 6.0 using 0.1 M HCl and NaOH solutions. The mixtures were shaken at 150 rpm at 25 °C for 1 h until the absorption process reached equilibrium. After magnetic separation, the adsorption capacity q_e was determined using FAAS.

2.5.4 Adsorption Selectivity

The selectivity of Cd(II)-IIP and Cd(II)-NIP toward Cd(II) ions and other metal ions was evaluated using a selectivity coefficient ($\beta^{2+2+}_{Cd/M}$), which was determined by incubating 5 mg of the adsorbent beads with heavy metal ions (at a concentration of 50 mg/L) in 10 mL of deionized water. The mixture was shaken at 150 rpm at 25 °C for 1 h. After magnetic separation, the distribution ratio (D) was calculated via FAAS using the following equation [35]:

$$D = \frac{V(C_0 - C_e)}{mC_e} \tag{3}$$

where, C_0 and C_e (mg/L) are the respective concentrations of metal ions in the initial and equilibrium solutions, V (L) is the volume of the aqueous solution, and m (g) is the mass of the dry beads. Meanwhile, the selectivity coefficient is defined as:

$$\beta_{Cd^{2+}/M^{2+}} = \frac{D_{Cd^{2+}}}{D_{M^{2+}}} \tag{4}$$

where, D^{2+}_{Cd} and D^{2+}_{M} are the distribution ratios of the Cd(II) ions and other co-existing metal ions, respectively. The effect of imprinting on the selective adsorption process was evaluated using the relative selectivity coefficient β_r, which is defined by the following equation:

$$\beta_r = \frac{\beta_{Cd(II)-IIP}}{\beta_{Cd(II)-NIP}} \tag{5}$$

where, $\beta_{Cd(II)\text{-}IIP}$ and $\beta_{Cd(II)\text{-}NIP}$ are the selective adsorption coefficient of Cd(II)-IIP and Cd(II)-NIP, respectively.

2.5.5 Desorption and Reusability

The desorption and regeneration of Cd(II)-IIP and Cd(II)-NIP toward Cd(II) ions was tested by adding 25 mg of either adsorbent into 50 mL of Cd(II) ion solution at a concentration of 100 mg/L, whose pH was adjusted to 6.0 using 0.1 M HCl and NaOH solutions. The mixture was shaken at 150 rpm and 25 °C for 1 h. After magnetic separation, the adsorption capacity (q_e) was determined using FAAS. The adsorbent was then filtered, and the Cd(II) ions were desorbed with 0.1 M HNO_3 aqueous solution by shaking over a period of 2 h. The adsorbent was washed thoroughly with deionized water to a neutral pH value. To test the reusability of the adsorbent, this adsorption–desorption cycle was repeated using the same adsorbent.

3 Results and Discussion

3.1 Characterization of AECS

The chemical structure of the synthesized AECS was characterized using ^{1}H NMR spectroscopy. AECS was dissolved in a mixed solvent system of CD_3COOD/D_2O (3:97), and the measurement was performed at room temperature. The ^{1}H NMR spectrum (Fig. 2) was used to analyse the AECS

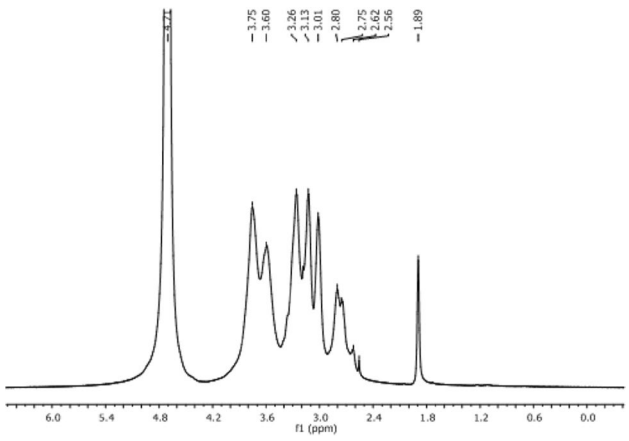

Fig. 2 ^{1}H-NMR (3% CD_3COOD/D_2O, 400 MHz) of AECS. δ (ppm): 1.89 (acetyl methyl), 2.60–3.20 (–$NHCH_2CH_2NH_2$), 3.26 (H-2), 3.60 (H-6a), 3.75 (H-3, 4, 5, 6b), 4.71 (H-1)

chemical structure. The chemical shift at $\delta = 1.89$ ppm was assigned to the proton of the residual acetyl methyl moiety, while the signal at $\delta = 2.60$–3.20 ppm revealed that the ethylamine substituent ($-NHCH_2CH_2NH_2$) was successfully modified. In addition, the signals between $\delta = 3.26$ and 4.71 ppm indicated the presence of sugar residues. The spectra were representative of the reaction product, and they were comparable to published literature [36]. In addition, the degree of deacetylation (DD) of AECS was established at 90%.

3.2 Characterization of Adsorbent

The Fe_3O_4, Fe_3O_4@SiO_2, Cd(II)-IIP, and Cd(II)-NIP particles were observed using a scanning electron microscope, and the results are shown in Fig. 3. Figure 3a–d shows that all four materials have a spherical morphology with a certain particle size distribution; the Fe_3O_4 and Fe_3O_4@SiO_2 particles have an average size of about 100 nm whereas the average particle size of Cd(II)-IIP in Fig. 3e and Cd(II)-NIP in Fig. 3d increased to about 30 µm owing to the chitosan-based modification. Figure 3f shows the loose surface structure of the Cd(II)-IIP adsorbent, which provides more active sites for free metal ions, thus improving the adsorption performance of the adsorbent.

CS, AECS, Fe_3O_4, Fe_3O_4@SiO_2, and Cd(II)-IIP were freeze-dried and compressed with KBr, before they were analyzed using a Vertex 70 Fourier transform infrared spectrometer in the scanning range of 400–4000 cm^{-1}. The IR spectra (Fig. 4) show the different absorption peaks at various wavelengths, i.e. the Fe–O stretching vibration peak at 581.32 cm^{-1} [37], Si–O-Si asymmetric stretching vibration peak at 1099.97 cm^{-1}, Si–O–Si symmetric stretching

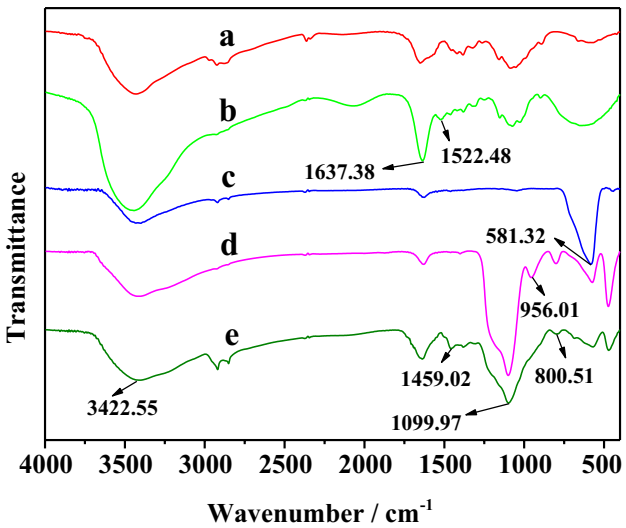

Fig. 4 FTIR spectra of CS (a), AECS (b), Fe_3O_4 (c), Fe_3O_4@SiO_2 (d) and Cd(II)-IPN (e)

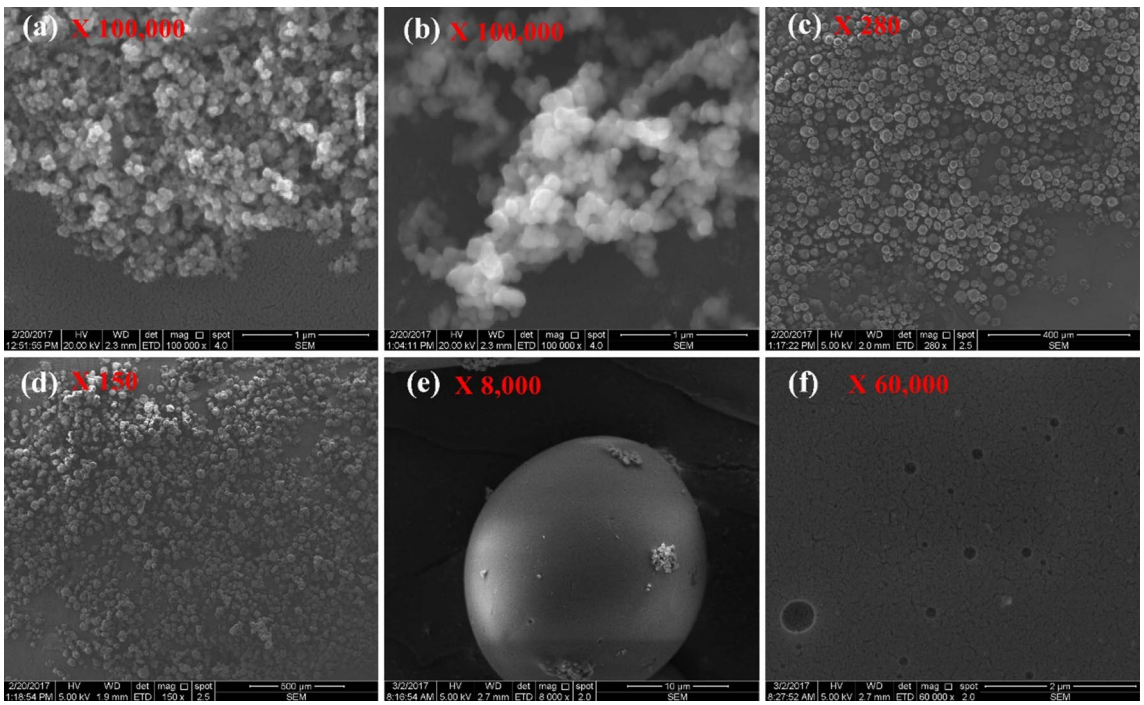

Fig. 3 SEM images of **a** Fe_3O_4 (×100,000); **b** Fe_3O_4@SiO_2 (×100,000); **c** Cd(II)-IIP (×280); **d** Cd(II)-NIP (×150); **e** Cd(II)-IIP (×8000); **f** Cd(II)-IIP (×60,000)

vibration peak at 800.51 cm^{-1}, Si–OH stretching vibration peak at 956.01 cm^{-1} [38, 39], O–H stretching vibration peak at 3422.55 cm^{-1}, the bending vibration peaks of $–NH_2$ and –NH– at 1522.48 cm^{-1} and 1459.02 cm^{-1}, respectively, as well as the stretching vibration peak of amide C=O at 1637.38 cm^{-1}. The appearance of these peaks indicated that AECS, Fe_3O_4, and $Fe_3O_4@SiO_2$ were successfully synthesized, and the modified chitosan was also successfully coated on the surface of $Fe_3O_4@SiO_2$.

About 10 mg each of powdered Fe_3O_4, $Fe_3O_4@SiO_2$, Cd(II)-IIP, and Cd(II)-NIP was placed in small crucibles and analyzed using a synchronous thermal analyzer. The heating rate was set at 10 °C/min, while the analyses were carried out in the temperature range of 50–800 °C. Figure 5 shows the thermo-gravimetric curves of these four samples. In the aforementioned temperature range, Fe_3O_4 and $Fe_3O_4@SiO_2$ showed a small amount of weight gain, which may be due to the oxidation of Fe_3O_4, raising the valency of iron from 8/3 to 3 while SiO_2 remained unchanged during the experiment; this led to an increase in the total sample quality. In the temperature range of 50–700 °C, the mass loss of Cd(II)-IIP and Cd(II)-NIP was nearly 70% owing to the decomposition of the sugar skeleton of AECS, as well as the evaporation of residual organic solvent in $Fe_3O_4@SiO_2$. When the temperature was increased to 600 °C, the organic matter was completely degraded. The residual red iron matter was Fe_2O_3.

About 10 mg each of powdered Fe_3O_4, $Fe_3O_4@SiO_2$, Cd(II)-IIP, and Cd(II)-NIP was analyzed using an X-ray diffractometer, which was operating at a tube voltage and tube current of 30 kV and 20 mA, respectively. Using a Cu-Kα irradiation source (λ = 0.15418·nm), the scanning process was performed in the range of 10–80° at a speed of 6 °C/min. Six main peaks were identified in the four respective materials, i.e. 2θ = 30.2°, 35.5°, 43.2°, 53.5°, 57.1°, and 62.7° (Fig. 6). The lattice parameters of (220), (311), (400), (422), (511), and (440) were determined based on the obtained XRD patterns using the MDI-JADE-6 program, and they corresponded to the magnetite crystal type (magnetite, JCPDS, No. 19-0619) [40, 41]. The analysis showed that $Fe_3O_4@SiO_2$, Cd(II)-IIP, and Cd(II)-NIP contained cubic Fe_3O_4, whose phase was kept unchanged during the synthetic process.

The magnetic properties of the magnetic absorbents directly influence their separation and recycling efficiency. The hysteresis loops of Fe_3O_4, $Fe_3O_4@SiO_2$, Cd(II)-IIP, and Cd(II)-NIP at room temperature (27 °C), which determine the main indicators of magnetic properties such as saturation magnetization (Ms), remanence (Mr), and coercivity (Hc), are shown in Fig. 7. The saturated magnetization values of Fe_3O_4, $Fe_3O_4@SiO_2$, Cd(II)-IIP, and Cd(II)-NIP were established at 82.6, 37.0, 14.3, and 13.3 emu/g, respectively. While the saturated magnetization of modified chitosan-coated Cd(II)-IIP and Cd(II)-NIP decreased significantly, both species could still quickly achieve solid–liquid separation in an external magnetic field. No remanence or coercivity were observed in the magnetic loop, thus proving that magnetic nanoparticles with superparamagnetic performance can be applied to magnetic separation [42].

The pelletizing ability of the adsorbents will directly affect their adsorption performance. Three main factors that influence balling performance have been identified: material ratio (1:1, 2:1, and 3:1 g/g; material ratio *m/m* = AECS/$Fe_3O_4@SiO_2$), cross-linking time (1, 2, and 3 h), and stirring speed (200, 300, and 400 rpm). They were used in a three-level orthogonal experiment to optimize experimental

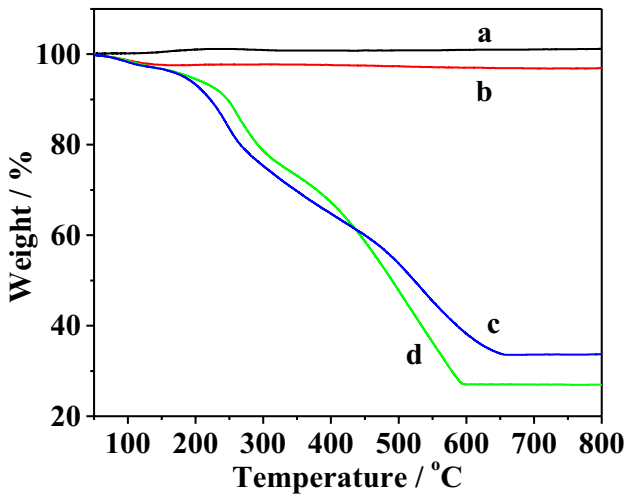

Fig. 5 TGA thermographs of Fe_3O_4 (a), $Fe_3O_4@SiO_2$ (b), Cd(II)-NIP (c) and Cd(II)-IIP (d)

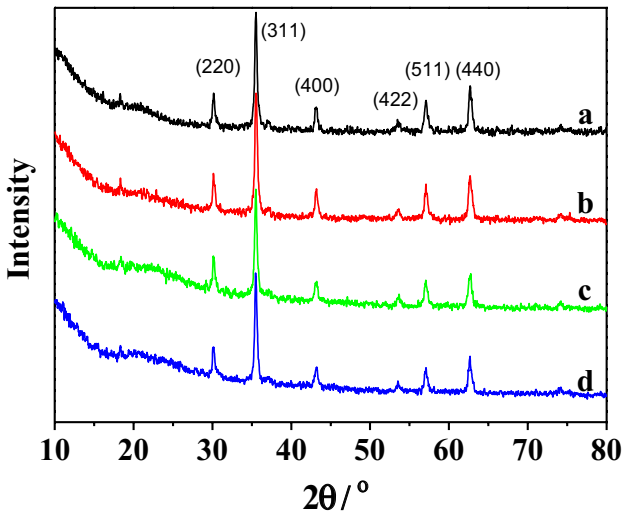

Fig. 6 XRD spectra of Fe_3O_4 (a), $Fe_3O_4@SiO_2$ (b), Cd(II)-NIP (c) and Cd(II)-IIP (d)

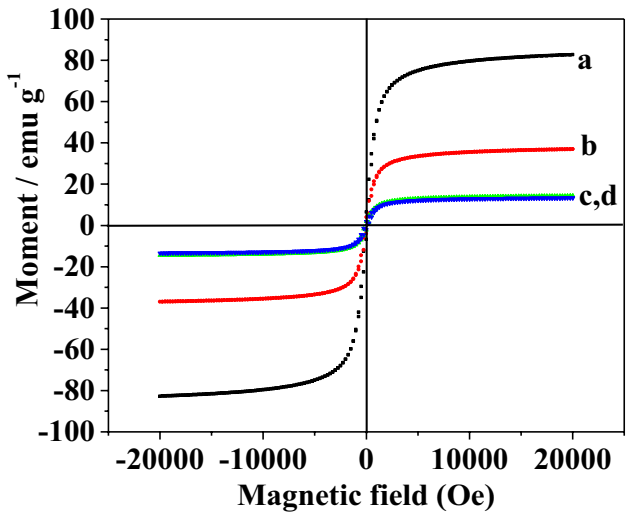

Fig. 7 Magnetic hysteresis curve of Fe_3O_4 (a), Fe_3O_4@SiO_2 (b), Cd(II)-IIP (c) and Cd(II)-NIP (d)

conditions. The synthesized particles were observed using an optical microscope, and their morphology was studied (Fig. 8).

Figure 8 shows that the microspheres were fragile when stirred at a speed of 400 rpm (Fig. 8-3, 5, 7) but reducing the stirring speed to 200 rpm resulted in slightly larger particles (Fig. 8-1, 6, 8). An increased ratio of AECS to Fe_3O_4@SiO_2 gave the products a deeper colour (Fig. 8-7, 8, 9). While cross-linking time had little influence on the ball formation, the optimal reaction time was found to be 1 h. As the microspheres shown in Fig. 8-4 and Fig. 8-9 are relatively small and uniform in size, the following experimental conditions—2:1 of AECS to Fe_3O_4@SiO_2, 1 h of cross-linking time, and a stirring speed of 300 rpm, were selected for all subsequent experiments.

3.3 Adsorption Experiments

3.3.1 Effect of pH

The pH value of the aqueous solution is an important parameter during the adsorption process. In this study, the influence of pH (in the range of pH 2–6) on the adsorption capacity of the adsorbents toward Cd(II) ions was studied. Figure 9 shows that the adsorption capacity gradually increased along with the pH value of the solution, reaching a maximum capacity at pH 6. The adsorption capacity of Cd(II)-IIP and Cd(II)-NIP toward Cd(II) ions at pH 6 were 24.2 and 6.3 mg/g, respectively. The $–CH_2–NH_2$ residues on the adsorbents are protonated in a highly acidic environment, thus forming a positively charged surface. This in turn obstructs the complexation of Cd(II) ions on the adsorbent materials. Owing to this competition with H_3O^+ ions, the adsorbents typically show low adsorption capacity

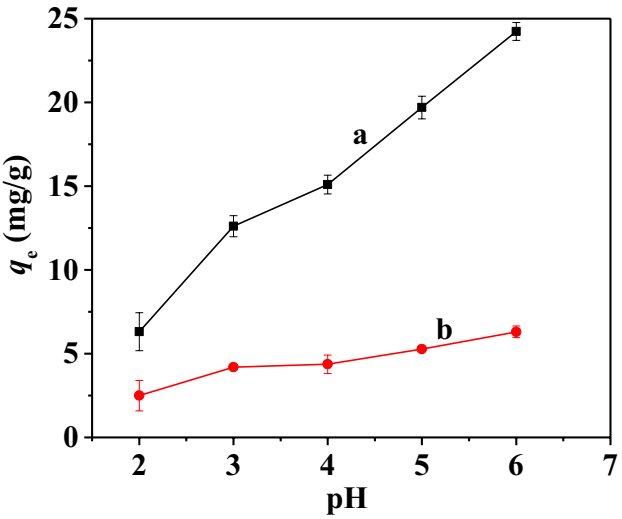

Fig. 9 Effect of pH values on adsorption capacity of heavy metal ions for Cd(II)-IIP (a) and Cd(II)-NIP (b)

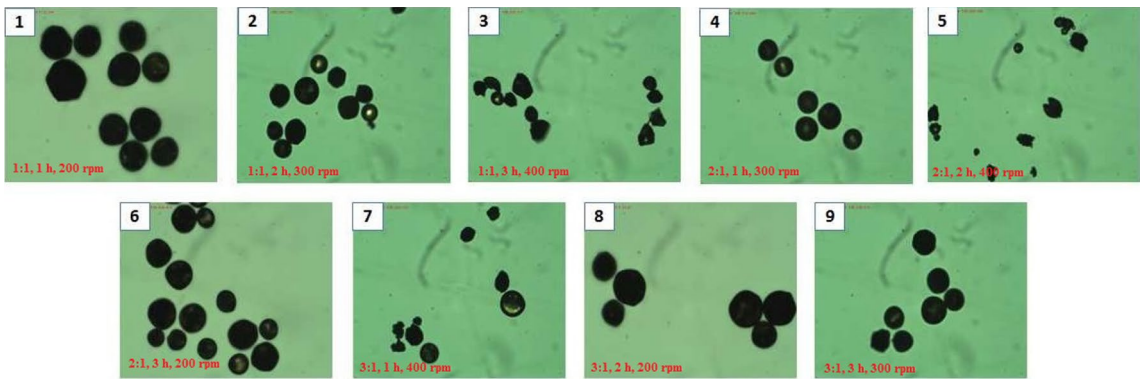

Fig. 8 Morphology of magnetic microspheres under microscope

at low pH values [43]. The solubility of positively charged Cd(II) ions decreases along with solution pH; When the pH value is higher than 6, Cd(II) ions easily undergo chemical precipitation and are not released into the solution, which then results in a decreased adsorption capacity of Cd(II)-IIP [44]. In addition, owing to the loose structure of the Cd(II)-IIP surface, the adsorption capacity of Cd(II)-IIP was about four times higher than that of Cd(II)-NIP, thus suggesting that the imprinting method is suitable for the Cd(II) ions adsorption process.

3.3.2 Adsorption Kinetics

Another important experimental parameter is the effect of time on the heavy metal adsorption process. Figure 10 shows the effect of contact time on the adsorption of Cd(II) ions using Cd(II)-IIP and Cd(II)-NIP. The adsorption rate increased sharply in the first 20 min, and subsequently stabilized within 60 min. The adsorption capacity of Cd(II)-IIP and Cd(II)-NIP toward Cd(II) ions were established at 24.9 and 6.4 mg/g, respectively. It is obvious that Cd(II)-IIP afforded a faster adsorption rate of Cd(II) ions compared to that of Cd(II)-NIP. This significant increase in the adsorption capacity of Cd(II)-IIP could be attributed to a large number of active sites on its surface, which can quickly adsorb Cd(II) ions from the solution. These results fully demonstrated that Cd(II)-IIP delivered a better performance for the adsorption of Cd(II) ions compared to Cd(II)-NIP. Nonetheless, both Cd(II)-IIP and Cd(II)-NIP could reach complete adsorption saturation in 60 min, with the imprinted cavities either staying exposed or being filled by Cd(II) ions. Based on these results, an adsorption time of 60 min was considered suitable for the sorption experiments.

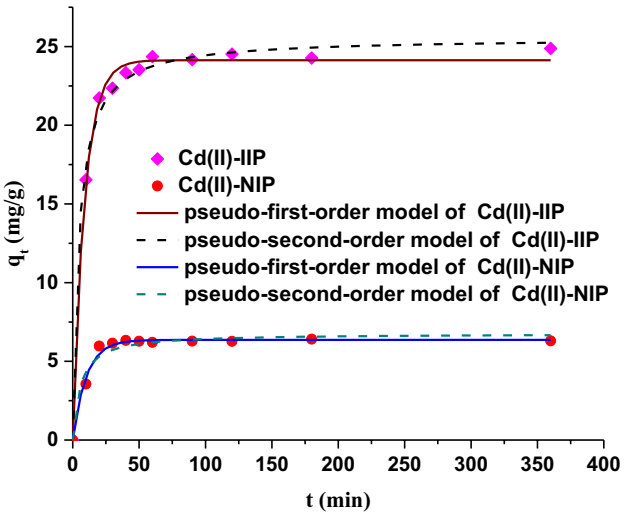

Fig. 10 Effect of time on the adsorption of Cd(II) ions using Cd(II)-IIP and Cd(II)-NIP

In order to investigate the kinetics of the Cd(II) adsorption process, its adsorption mechanism and rate determining step were studied by employing the pseudo-first-order and pseudo-second-order kinetic models.

The pseudo-first-order model is expressed by the following equation [45]:

$$q_t = q_e(1 - e^{K_1 t}) \tag{6}$$

Meanwhile, the pseudo-second-order model is defined as [46]:

$$q_t = \frac{K_2 q_e^2 t}{1 + K_2 q_e t} \tag{7}$$

where, K_1 and K_2 (min^{-1}) are the pseudo-first-order and pseudo-second-order rate constants, respectively, q_e (mg/g) is the adsorption capacity at equilibrium, and q_t (mg/g) is the amount of ions adsorbed at time t.

The linear fitting curves of the two models and the kinetic parameters are shown in Fig. 10 and Table 1. As seen in Table 1, the correlation coefficient (R^2) values of Cd(II)-IIP and Cd(II)-NIP according to the pseudo-first-order and pseudo-second-order models were close to 1.000. The q_e value calculated from the pseudo-second-order model was close to the experimental data. It was proven that chemisorption was the rate controlling step, which involves chemical bonding between divalent metal ions and polar functional groups (–NH_2 and –OH) on the adsorbent [47]. It was reported that Cd(II) ions could be coordinated with N and O atoms to obtained octahedral cadmium coordinations or five-membered chelate rings [48, 49], and the chelating effect could benefit the adsorption of AECS on the Cd(II)-IIP.

3.3.3 Adsorption Isotherm

Adsorption isotherms are used to describe the relationship between equilibrium adsorption capacities and the amounts of adsorbate adsorbed on adsorbent at a constant

Table 1 Kinetic parameters of the adsorption models using Cd(II)-IIP and Cd(II)-NIP as adsorbents

	Cd(II)-IIP	Cd(II)-NIP
Measured q_e (mg/g)	24.9	6.4
Pseudo-first-order model		
q_e (theory) (mg/g)	24.1	6.4
K_1 (min^{-1})	0.111	0.098
R^2	0.996	0.987
Pseudo-second-order model		
q_e (theory) (mg/g)	25.6	6.8
K_2 (min^{-1})	0.009	0.028
R^2	0.994	0.957

temperature. To investigate the adsorption isotherms, two classical equilibrium models known as the Langmuir and Freundlich models were used.

The Langmuir isotherm equation is defined as [50]:

$$\frac{C_e}{q_e} = \frac{1}{bQ_m} + \frac{C_e}{Q_m} \tag{8}$$

Meanwhile, the Freundlich isotherm equation is expressed as [51]:

$$q_e = K_f C_e^{1/n} \tag{9}$$

where, q_e (mg/g) is the adsorption capacity at equilibrium, C_e (mg/L) is the equilibrium concentration, Q_m (mg/g) is the maximum adsorption capacity, b (L/mg) is the Langmuir adsorption equilibrium constant, K_f (mg/g (L/mg)$^{1/n}$) is the Freundlich adsorption equilibrium constant, and n is the adsorption intensity constant.

Results comparing the two models based on non-linear fitting and their adsorption isotherm parameters are shown in Fig. 11 and Table 2. In Table 2, the adsorption behaviour of Cd(II) ions on Cd(II)-IIP and Cd(II)-NIP agreed better with the Langmuir model as evidenced by higher R^2 values (0.994 and 0.976), thus demonstrating that a homogeneous monolayer of AECS was bound on the surface of the imprinted and non-imprinted adsorbents [52].

According to the Langmuir model, the maximum adsorption capacities of Cd(II)-IIP and Cd(II)-NIP toward Cd(II) ions were 26.1 and 6.7 mg/g, respectively, which were close to the measured values 25.2 and 6.4 mg/g (Table 2). The correlation coefficient of the Langmuir model was approximately 1, indicating that it was better than the Freundlich model. In addition, the separation factor (b) value of 0.116 indicated that Cd(II)-IIP could be suitably used for the adsorption of Cd(II) ions in aqueous solutions [53]. The maximum adsorption capacities of Cd(II) ions in different adsorbents are included in Table 3. It can be seen that the adsorption performance of Cd(II)-IIP is better than some reported adsorbents including activated carbons, resins, and biomass materials, but it is still lower than other commercial adsorbents. However, Cd(II)-IIP showed obvious selectivity for Cd(II) ions which makes it promising adsorbent for the selective removal of Cd(II) ions from aqueous solutions.

3.4 Adsorption Selectivity

In order to study the selectivity of the Cd(II)-IIP adsorbent toward Cd(II) ions, Cu(II), Cr(II), and Pb(II) ions (which

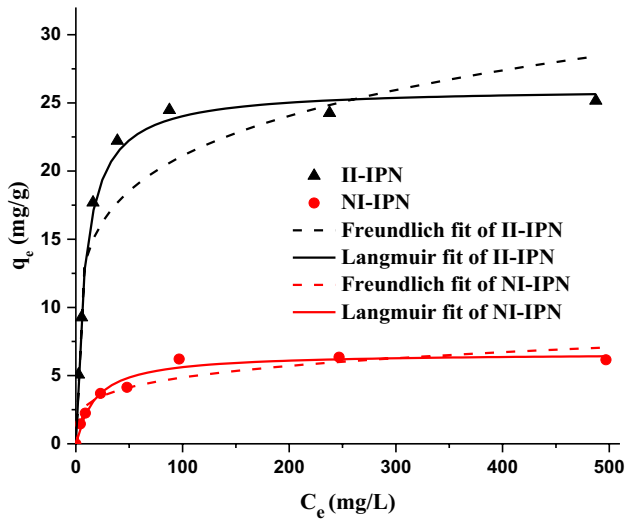

Fig. 11 Effect of the equilibrium concentration of Cd(II) ions on adsorption using Cd(II)-IIP and Cd(II)-NIP

Table 3 The maximum adsorption capacities comparison of Cd(II) ions

Adsorbent	Cd(II) Q_m (mg/g)	Reference
Cd(II)-IIP	26.1	This work
Cd(II)-NIP	6.7	This work
Activated carbon (hazelnut husks)	20.9	[54]
Activated carbon (Olive stone waste)	7.8	[55]
Thiosemicarbazide-grafted multi-walled carbon nanotubes	3.69	[56]
Carbon aerogel	15.53	[57]
Powdered activated carbon (PAC)	32.89	[58]
Purolite AC 20	12.64	[59]
Biochar (Coaltec Energy, USA Inc.)	33.90	[59]
Lewatit TP 207 resin	50.0	[60]
D2EHPA-impregnated XAD7 resin	4.5	[61]
Lignocellulosic residues BOP	10.5	[20]
Palm oil boiler mill fly ash (POFA)	15.82	[62]
Activated sludge	9.6	[63]

Table 2 Adsorption isotherm parameters using Cd(II)-IIP and Cd(II)-NIP as adsorbents

Type	Measured value q_e (mg/g)	Langmuir model			Freundlich model		
		Q_m (mg/g)	B (L/mg)	R^2	$1/n$	K_F (mg/g)(L/mg)$^{1/n}$	R^2
Cd(II)-IIP	25.2	26.1	0.116	0.994	0.187	8.91	0.865
Cd(II)-NIP	6.4	6.7	0.054	0.976	0.234	1.66	0.902

have an identical charge and are similar in size to Cd(II) ions) were chosen as competitor ions. Table 4 lists the adsorption parameters of the tested binary systems, which include distribution ratio, selectivity coefficients, and relative selectivity coefficients.

Our results showed that the distribution ratio of Cd(II) ions for the Cd(II)-IIP adsorbent was 3–5 times that of Cd(II)-NIP. In contrast, the distribution ratio of other competitor ions for Cd(II)-IIP was only 1–2 times that of Cd(II)-NIP. It is evident that Cd(II)-NIP was not selective toward Cd(II) ions as it showed a higher adsorption selectivity toward competitor ions as opposed to the Cd(II) species. Using the imprinting technique, the adsorption selectivity of Cd(II)-NIP can be improved. The relative selectivity coefficients βr of the tested binary systems were all larger than two, thus indicating that the selective adsorption of the non-imprinted adsorbent was significantly improved post modification.

These results suggested that Cd(II)-IIP contains imprinted cavities and specific binding sites that exist in a predetermined orientation, and they are specific to Cd(II) ions as Cu(II), Cr(II), and Pb(II) ions fit poorly into the Cd(II)-imprinted cavity. Owing to specific hole recognition toward Cd(II) ions on the surface of Cd(II)-IIP, more template ions from the binary system are trapped and this leads to a higher adsorption capacity of the adsorbent. Therefore, using the imprinting method to fabricate the Cd(II)-IIP adsorbent will impart a high recognition ability and high selectivity toward Cd(II) ions.

3.5 Regeneration Study

In order to improve the process economics of using Cd(II)-IIP for practical applications, it is important to establish the stability and reusability of the adsorbent. As it has poor adsorption properties under low pH conditions, 0.1 M HNO_3 solution was chosen as a desorption agent. As shown in Fig. 12, the adsorption performance of Cd(II)-IIP dropped to 74% after undergoing six cycles of the adsorption–desorption process. Even though Cd(II) ions were fixed on the adsorbent surface and could not be completely eluted, the adsorbent still showed a decent degree of recycling potential.

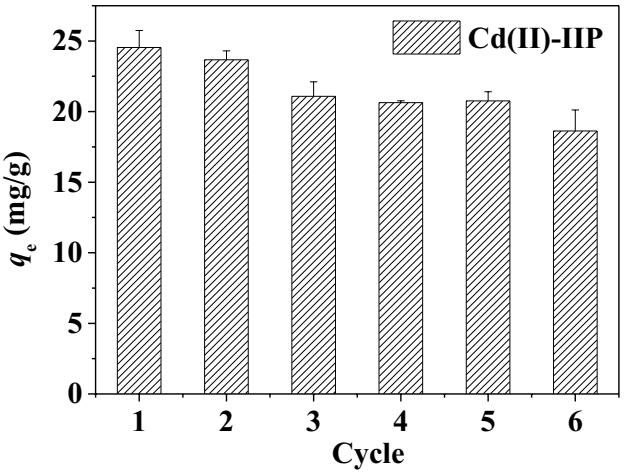

Fig. 12 Regeneration of Cd(II)-IIP

4 Conclusions

Using the ion-imprinting technique, a novel magnetic adsorbent Fe_3O_4@SiO_2@AECS was successfully prepared, and it demonstrated selective adsorption behaviour toward Cd(II) ions. To study the changes that occur during the chemical modification and Cd(II) ion-imprinting processes, the synthesized materials were analyzed using various analytical techniques, including FTIR, NMR, VSM, SEM, TGA, XRD, and FAAS. The results showed that the adsorbents have small particle size, loose surface structure, and excellent magnetic response, properties that are ideal for heavy metal ion adsorption.

The ion-imprinted adsorbent Cd(II)-IIP and the non-imprinted adsorbent Cd(II)-NIP were tested in a series of batch experiments to evaluate the experimental parameters that affect the selective adsorption of Cd(II) ions. The observed experimental adsorption data agreed with the Langmuir isotherm model. In addition, the adsorption

Table 4 Parameters of adsorption selectivity in binary mixtures

Binary mixture	Ions	Distribution ratio D (mL/g)		Selectivity coefficient $\beta^{2+2+}_{Cd/M}$		Relative selectivity coefficient β_r
		Cd(II)-IIP	Cd(II)-NIP	Cd(II)-IIP	Cd(II)-NIP	
Cd^{2+}/Cu^{2+}	Cd^{2+}	231.92	51.51	2.188	0.660	3.315
	Cu^{2+}	106.01	78.02			
Cd^{2+}/Cr^{2+}	Cd^{2+}	268.47	60.58	1.926	0.497	3.875
	Cr^{2+}	139.40	121.89			
Cd^{2+}/Pb^{2+}	Cd^{2+}	307.32	99.41	1.381	0.670	2.061
	Pb^{2+}	222.57	148.32			

kinetics appeared to conform to the pseudo-first or second-order model. The maximum adsorption capacity of Cd(II)-IIP (26.1 mg/g) was higher than that of Cd(II)-NIP (6.4 mg/g), and Cd(II)-IIP also had better selectivity toward Cd(II) ions in binary solution systems. Results from the regeneration test of AECS showed that the adsorption performance of Cd(II)-IIP fell to 74% after six adsorption–desorption cycles.

Acknowledgements We are grateful to the National Natural Science Foundation of China (Grant No. 41771509), Zhejiang Science and Technology Project (Grant Nos. 2018C37052, 2016C37078, 2008C14067) and SRF for ROCS, SEM.

References

1. F. Fu, Q. Wang, Removal of heavy metal ions from wastewaters: a review. J. Environ. Manag. **92**(3), 407–418 (2011)
2. S.A. Abo-El-Enein, M.A. Eissa, A.A. Diafullah, M.A. Rizk, F.M. Mohamed, Removal of some heavy metals ions from wastewater by copolymer of iron and aluminum impregnated with active silica derived from rice husk ash. J. Hazard. Mater. **172**(2–3), 574–579 (2009)
3. W.S. Wan Ngah, M.A. Hanafiah, Removal of heavy metal ions from wastewater by chemically modified plant wastes as adsorbents: a review. Bioresour. Technol. **99**(10), 3935–3948 (2008)
4. S. Squadrone, M. Prearo, P. Brizio, S. Gavinelli, M. Pellegrino, T. Scanzio, S. Guarise, A. Benedetto, M.C. Abete, Heavy metals distribution in muscle, liver, kidney and gill of European catfish (*Silurus glanis*) from Italian Rivers. Chemosphere **90**(2), 358–365 (2013)
5. A. Bernard, Renal and Neurological Effects Heavy Metals in the Environment. Encycl Environ Health (2011). https://doi.org/10.1016/B978-0-444-52272-6.00615-2
6. M. Vigeh, K. Yokoyama, A.A. Shinohara, M. Afshinrokh, Increase in blood heavy metals in early pregnancy induce hypertension in pregnant women. Toxicol. Lett. **205**, 197–197 (2011)
7. M. Kumar, B.P. Tripathi, V.K. Shahi, Crosslinked chitosan/polyvinyl alcohol blend beads for removal and recovery of Cd(II) from wastewater. J. Hazard. Mater. **172**(2–3), 1041–1048 (2009)
8. Y. Xi, Y. Luo, J. Luo, X. Luo, Removal of cadmium(II) from wastewater using novel cadmium ion-imprinted polymers. J. Chem. Eng. Data **60**(11), 3253–3261 (2015)
9. L.P. Lingamdinne, Y.Y. Chang, J.K. Yang, J. Singh, E.H. Choi, M. Shiratani, J.R. Koduru, P. Attri, Biogenic reductive preparation of magnetic inverse spinel iron oxide nanoparticles for the adsorption removal of heavy metals. Chem. Eng. J. **307**, 74–84 (2017)
10. J.K. Bediako, W. Wei, S. Kim, Y.S. Yun, Removal of heavy metals from aqueous phases using chemically modified waste Lyocell fiber. J. Hazard. Mater. **299**, 550–561 (2015)
11. M.I. Shariful, S.B. Sharif, J.J.L. Lee, U. Habiba, B.C. Ang, M.A. Amalina, Adsorption of divalent heavy metal ion by mesoporous-high surface area chitosan/poly (ethylene oxide) nanofibrous membrane. Carbohydr. Polym. **157**, 57–64 (2017)
12. C. Ren, X. Ding, W. Li, H. Wu, H. Yang, Highly efficient adsorption of heavy metals onto novel magnetic porous composites modified with amino groups. J. Chem. Eng. Data **62**, 1865–1875 (2017)
13. D. Mohan, C.U. Pittman Jr., Activated carbons and low cost adsorbents for remediation of tri- and hexavalent chromium from water. J. Hazard. Mater. **137**(2), 762–811 (2006)
14. G. Crini, Recent developments in polysaccharide-based materials used as adsorbents in wastewater treatment. Prog. Polym. Sci. **30**(1), 38–70 (2005)
15. A. Kucinska, A. Cyganiuk, J.P. Lukaszewicz, A microporous and high surface area active carbon obtained by the heat-treatment of chitosan. Carbon **50**(8), 3098–3101 (2012)
16. X. Sun, Q. Li, L. Yang, H. Liu, Removal of chromium(VI) from wastewater using weakly and strongly basic magnetic adsorbents: adsorption/desorption property and mechanism comparative studies. RSC Adv. **6**, 18471–18482 (2016)
17. K. El-Tahlawy, R. Venditti, J. Pawlak, Effect of alkyl ketene dimer reacted starch on the properties of starch microcellular foam using a solvent exchange technique. Carbohydr. Polym. **73**, 133–142 (2008)
18. A. Petrella, V. Petruzzelli, E. Ranieri, V. Catalucci, D. Petruzzelli, Sorption of Pb(II), Cd(II) and Ni(II) from single- and multimetal solutions by recycled waste porous glass. Chem. Eng. Commun. **203**(7), 940–947 (2016)
19. P. Rodríguezestupiñán, A. Erto, L. Giraldo, J.C. Morenopirajáan, Adsorption of Cd (II) on modified granular activated carbons: isotherm and column study. Molecules **22**(12), 2280 (2017)
20. A. Petrella, D. Spasiano, P. Acquafredda, N. De Vietro, E. Ranieri, P. Cosma, V. Rizzi, V. Petruzzelli, D. Petruzzelli, Heavy metals retention (Pb(II), Cd (II), Ni (II)) from single and multimetal solutions by natural biosorbents from the olive oil milling operations. Process. Saf. Environ. **114**, 79–90 (2018)
21. M. Hua, S. Zhang, B. Pan, W. Zhang, L. Lv, Q. Zhang, Heavy metal removal from water/wastewater by nanosized metal oxides: a review. J. Hazard. Mater. **211–212**, 317–331 (2012)
22. M.A. El-Sayed, Some interesting properties of metals confined in time and nanometer space of different shapes. Acc. Chem. Res. **32**, 257–264 (2001)
23. Y. Cao, L. Wen, F. Svec, T. Tan, Y. Lv, Magnetic AuNP@Fe_3O_4, nanoparticles as reusable carriers for reversible enzyme immobilization. Chem. Eng. J. **286**, 272–281 (2016)
24. A.S. de Dios, M.E. Diaz-Garcia, Multifunctional nanoparticles: analytical prospects. Anal. Chim. Acta **666**(1–2), 1–22 (2010)
25. K. Zargoosh, H. Abedini, A. Abdolmaleki, M.R. Moldavians, Effective removal of heavy metal ions from industrial wastes using thiosalicylhydrazide-modified magnetic nanoparticles. Ind. Eng. Chem. Res. **52**, 14944–14954 (2013)
26. Y.C. Lin, H.P. Wang, F. Gohar, M.H. Ullah, X. Zhang, D.F. Xie, H. Fang, J. Huang, J.X. Yang, Preparation and copper ions adsorption properties of thiosemicarbazide chitosan from squid pens. Int. J. Biol. Macromol. **95**, 476–483 (2017)
27. Y. Ren, X. Wei, M. Zhang, Adsorption character for removal Cu(II) by magnetic Cu(II) ion imprinted composite adsorbent. J. Hazard. Mater. **158**(1), 14–22 (2008)
28. S. Cen, W. Li, S. Xu, Z. Wang, Y. Tang, H. Wang, C. Wei, Application of magnetic Cd^{2+} ion-imprinted mesoporous organosilica nanocomposites for mineral wastewater treatment. RSC Adv. **7**, 7996–8003 (2017)
29. J. Huang, H. Xie, S. Hu, T. Xie, J. Gong, C. Jiang, Q. Ge, Y. Wu, S. Liu, Y. Cui, J. Mao, L. Mei, Preparation, characterization, and biochemical activities of N-(2-carboxyethyl)chitosan from squid pens. J. Agric. Food Chem. **63**, 2464–2471 (2015)
30. J.Y. Je, S.K. Kim, Antimicrobial action of novel chitin derivative. Biochim. Biophys. Acta **1760**, 104–109 (2006)
31. X.Q. Liu, J.M. Xing, Y.P. Guan, G.B. Shan, H.Z. Liu, Synthesis of amino-silane modified superparamagnetic silica supports and their use for protein immobilization. Colloids Surf. A **238**, 127–131 (2004)
32. W. Stöber, A. Fink, E. Bohn, Controlled growth of monodisperse silica spheres in the micron size range. J. Colloid Interface Sci. **26**, 62–69 (1968)

33. A. Hirai, H. Odani, A. Nakajima, Determination of degree of deacetylation of chitosan by ^{1}H NMR spectroscopy. Polym. Bull. **26**, 87–94 (1991)
34. A.A. Ehab, A.T. Dina, Y.N. Mostafa, A tunable template-assisted hydrothermal synthesis of hydroxysodalite zeolite nanoparticles using various aliphatic organic acids for the removal of zinc(II) ions from aqueous media. J. Inorg. Organomet. Polym Mater. **29**(1), 229–249 (2019)
35. B. Liu, X. Lv, X. Meng, G. Yu, D. Wang, Removal of Pb(II) from aqueous solution using dithiocarbamate modified chitosan beads with Pb(II) as imprinted ions. Chem. Eng. J. **220**, 412–419 (2013)
36. E.J. Dunn, X. Zhang, D. Sun, M.F.A. Goosen, Synthesis of N-(aminoalkyl) chitosan for microcapsules. J. Appl. Polym. Sci. **50**, 353–365 (2010)
37. Z. Xu, Y. Feng, X. Liu, M. Guan, C. Zhao, H. Zhang, Synthesis and characterization of Fe_3O_4@SiO_2@poly-L-alanine, peptide brush-magnetic microspheres through NCA chemistry for drug delivery and enrichment of BSA. Colloids Surf. B **81**, 503–507 (2010)
38. L. Wang, Y. Sun, J. Wang, A. Yu, H. Zhang, D. Dong, Preparation of surface plasmon resonance biosensor based on magnetic core/shell Fe_3O_4/SiO_2 and $Fe_3O_4/Ag/SiO_2$ nanoparticles. Colloids Surf. B **84**, 484–490 (2011)
39. D. Shao, K. Xu, X. Song, J. Hu, W. Yang, C. Wang, Effective adsorption and separation of lysozyme with PAA-modified Fe_3O_4@silica core/shell microspheres. J. Colloid Interface Sci. **336**, 526–532 (2009)
40. I.F. Nata, G.W. Salim, C.K. Lee, Facile preparation of magnetic carbonaceous nanoparticles for Pb^{2+} ions removal. J. Hazard. Mater. **183**(1–3), 853–858 (2010)
41. Y. Zhang, X. Liu, J. Nie, L. Yu, Y. Zhong, C. Huang, Improve the catalytic activity of α-Fe_2O_3, particles in decomposition of ammonium perchlorate by coating amorphous carbon on their surface. J. Solid State Chem. **184**, 387–390 (2011)
42. A. Dolgormaa, C.J. Lv, Y. Li, J. Yang, J.X. Yang, P. Chen, H.P. Wang, J. Huang, Adsorption of Cu(II) and Zn(II) Ions from Aqueous Solution by Gel/PVA-Modified Super-Paramagnetic Iron Oxide Nanoparticles. Molecules **23**(11), 2982 (2018)
43. Buhani, Narsito, Nuryono, E.S. Kunarti, Production of metal ion imprinted polymer from mercapto-silica through so-gel process as selective adsorbent of cadmium. Desalination **251**, 83–89 (2010)
44. A. Aklil, M. Mouflih, S. Sebti, Removal of heavy metal ions from water by using calcined phosphate as a new adsorbent. J. Hazard. Mater. **112**, 183–190 (2004)
45. Buhani, Suharso, Sumadi, Adsorption kinetics and isotherm of Cd(II) ion on Nannochloropsis sp biomass imprinted ionic polymer. Desalination **259**, 140–146 (2010)
46. Y.S. Ho, Second-order kinetic model for the sorption of cadmium onto tree fern: a comparison of linear and non-linear methods. Water Res. **40**, 119–125 (2006)
47. Y.S. Ho, G. Mckay, A comparison of chemisorption kinetic models applied to pollutant removal on various sorbents. Process Saf. Environ. **76**, 332–340 (1998)
48. Z. Popovii, G. Pavlovii, M. Vinkovii, D. Vikiivii, M.R. Linarii, Coordination modes of 3-hydroxypicolinic acid (OH-picH): synthesis and characterization of cadmium(II) complexes. Crystal and molecular structures of $[CdX(OH\text{-}pic)(OH\text{-}picH)(H_2O)]_2$ X = Cl^-, Br^-. Polyhedron **25**(12), 2353–2362 (2006)
49. C.W. Belock, A. Cetin, N.V. Barone, C.J. Ziegler, Transition Metal Coordination Chemistry of N, N-Bis(2-{pyrid-2-ylethyl}) hydroxylamine. Inorg. Chem. **47**(16), 7114–7120 (2008)
50. H. Soltani, A. Belmokhar, F.Z. Zeggal, A. Benyoucef, S. Bousalem, K. Bachari, Copper(II) removal from aqueous solutions by PANI-clay hybrid material: fabrication, characterization, adsorption and kinetics study. J. Inorg. Organomet. Polym. Mater. (2019). https://doi.org/10.1007/s10904-018-01058-z
51. B. Zhang, Y. Wu, Y. Fan, Synthesis of Novel Magnetic $NiFe_2O_4$ Nanocomposite Grafted Chitosan and the Adsorption Mechanism of Cr(VI). J. Inorg. Organomet. Polym Mater. **29**, 290–301 (2019)
52. M.H. Karaoglu, S. Zor, M. Ugurlu, Biosorption of Cr(III) from solutions using vineyard pruning waste. Chem. Eng. J. **159**, 98–106 (2010)
53. Y. Liu, X. Hu, M. Meng, Z. Liu, L. Ni, X. Meng, J. Qiu, RAFT-mediated microemulsion polymerization to synthesize a novel high-performance graphene oxide-based cadmium imprinted polymer. Chem. Eng. J. **302**, 609–618 (2016)
54. M. Imamoglu, Adsorption of Cd(II) Ions onto activated carbon prepared from hazelnut husks. J. Disper. Sci. Technol. **34**(9), 1183–1187 (2013)
55. T.M. Alslaibi, I. Abustan, M.A. Ahmad, A.A. Foul, Kinetics and equilibrium adsorption of iron (II), lead (II), and copper (II) onto activated carbon prepared from olive stone waste. Desalin. Water Treat. **52**(40–42), 7887–7897 (2014)
56. J. Zhang, Preparation, characterization and application of thiosemicarbazide grafted multiwalled carbon nanotubes for solid-phase extraction of Cd(II), Cu(II) and Pb(II) in environmental samples. J. Environ. Sci. **25**(11), 2331–2337 (2013)
57. J. Goel, K. Kadirvelu, A.C. Rajagopal, V.K. Garg, Cadmium(II) Uptake from aqueous solution by adsorption onto carbon aerogel using a response surface methodological approach. Ind. Eng. Chem. Res. **45**(19), 6531–6537 (2006)
58. K. Yang, J. Fox, DPF soot as an adsorbent for Cu(II), Cd(II), and Cr(VI) compared with commercial activated carbon. Environ. Sci. Pollut. Res. **25**(9), 8620–8635 (2018)
59. D. Kołodyńska, J. Krukowska, P. Thomas, Comparison of sorption and desorption studies of heavy metal ions from biochar and commercial active carbon. Chem. Eng. J. **307**, 353–363 (2017)
60. P. Brown, I.A. Jefcoat, D. Parrish, S. Gill, E. Graham, Evaluation of the adsorptive capacity of peanut hull pellets for heavy metals in solution. Adv. Environ. Res. **4**(1), 19–29 (2000)
61. M. Ciopec, C. Davidescu, A. Negrea, L. Lupa, P. Negrea, A. Popa, C. Muntean, Use of D2EHPA-impregnated XAD7 resin for the removal of Cd(II) and Zn(II) from aqueous solutions. Environ. Eng. Manag. J. **10**(10), 1597–1608 (2011)
62. A.S.A. Aziz, L.A. Manaf, H.C. Man, N.S. Kumar, Equilibrium studies and dynamic behavior of cadmium adsorption by palm oil boiler mill fly ash (POFA) as a natural low-cost adsorbent. Desalin. Water Treat. **54**(7), 1956–1968 (2015)
63. S.A. Ong, M. Hirata, T. Hano, Comparative study on kinetic adsorption of Cu(II), Cd(II) and Ni(II) ions from aqueous solutions using activated sludge and dried sludge. Appl. Water Sci. **3**(1), 321–325 (2013)

Publisher's Note Springer Nature remains neutral with regard to jurisdictional claims in published maps and institutional affiliations.